Electronic States and Optical Properties of Porphyrins in van der Waals Contact: Th^{IV} Sandwich Complexes

Osman Bilsel,[†] Juan Rodriguez,[†,‡] Stanley N. Milam,[§,⊥] Philip A. Gorlin,[§] Gregory S. Girolami,*[,§] Kenneth S. Suslick,*[,§] and Dewey Holten*[,†]

Contribution from the Department of Chemistry, Washington University, St. Louis, Missouri 63130, and School of Chemical Sciences, University of Illinois at Champaign-Urbana, Urbana, Illinois 61801. *Received January 31, 1992*

Abstract: Ground-state and time-resolved excited-state absorption spectra and fluorescence and phosphorescence spectra of three Th^{IV} sandwich complexes, $Th^{IV}(TPP)_2$, $Th^{IV}(OEP)_2$, and $Th^{IV}(OEP)(TPP)$, are reported (OEP = 2,3,7,8,12,13,17,18-octaethylporphyrinate, TPP = 5,10,15,20-tetraphenylporphyrinate). These complexes, in which the nitrogen planes of the two porphyrin macrocycles are ~2.9 Å apart, exhibit a number of prominent optical characteristics: (i) monoporphyrin-like Q and B absorption bands, (ii) a new absorption between the Q and B bands, (iii) a weak, low-energy absorption that is substantially red-shifted relative to the Q bands of analogous monoporphyrin complexes, (iv) fluorescence and phosphorescence emission bands that are even further red-shifted relative to typical emission bands from porphyrin monomers, and (v) a moderately intense near-infrared $^3(\pi,\pi^*)$ excited-state absorption not observed in monomeric porphyrins. These characteristic optical properties of the sandwich complexes are all accounted for by a relatively simple molecular orbital configuration-interaction model. Additionally, the spectral data and molecular orbital model identify the energies of charge-transfer configurations and delineate their contribution to the electronic states of these strongly-coupled π systems. These results provide insights into the interactions that can take place between other pairs of chromophores brought within van der Waals contact, such as the bacteriochlorophyll dimer of the photosynthetic reaction center.

Introduction

Investigations of cofacial porphyrin dimers have been motivated by an effort to better understand and mimic the interactions within the dimeric primary electron donor of the photosynthetic reaction center. The two bacteriochlorophyll molecules of the C_2-symmetry "special pair" are separated by ~3.3 Å.[1] Electronic interactions within this dimer are thought to be responsible for some of its characteristic properties, such as the ease of porphyrin π-system oxidation and the low energy of the first $^1(\pi,\pi^*)$ excited state compared to corresponding monomeric chromophores. The latter property produces a bathochromic shift in the long-wavelength absorption band and makes the dimer an effective trap for the harvested photon energy.

Many factors might contribute to the origin of the electronic properties of the special pair. For example, the relative importance of exciton (i.e., dipole–dipole) coupling of the lowest excited states of the bacteriochlorophyll subunits, versus mixing with charge-transfer (CT) configurations, versus energy shifts from protein effects has yet to be established.[2,3] The energies of the CT configurations of the special pair (and of dimers in general) are not known and are expected to depend strongly on the interactions between the subunits. Hence, deducing the contribution of CT configurations to the lowest electronic states of a dimer is intimately related to understanding the degree of intermacrocycle orbital overlap.

Recently, several bis(porphyrin) sandwich complexes have been described whose optical characteristics resemble those of the lowest excited states to the special pair[2-4] and other dimers, such as aromatic excimers[5] and paracyclophanes.[6] The sandwich complexes also offer advantages as probes of π–π interactions. For example, the separation of the π systems can be tuned in fine (~0.1 Å) increments via the choice of the central metal ion. In this manner, the mean separation between the nitrogen planes of the two porphyrin subunits can be varied from ~2.9 Å for Th,[7] to ~2.8 Å for Ce,[8] and to ~2.6 Å for Zr and Hf,[9,10] with a mean separation between the core atoms of the two π systems varying correspondingly from ~3.5 to 3.2 Å.

The sandwich complexes show optical characteristics that are *not* exhibited by porphyrin dimers having larger separations between the macrocycles. These characteristics include a broad absorption 1000–3000 cm^{-1} to the red of the $^1Q(\pi,\pi^*)$ absorption of monoporphyrins,[7-15] a broad weak fluorescence substantially

[†] Washington University.
[‡] Present address: Department of Physics, Centenary College, Shreveport, LA 71134.
[§] University of Illinois at Champaign-Urbana.
[⊥] Present address: Shell Development Co., Houston, TX 77082.

(1) (a) Deisenhofer, J.; Epp, O.; Miki, K.; Huber, R.; Michel, H. *J. Mol. Biol.* **1984**, *180*, 385-398. (b) Yeates, T. O.; Komiya, H.; Chirino, A.; Rees, D. C.; Allen, J. P.; Feher, G. *Proc. Natl. Acad. Sci. U.S.A.* **1988**, *85*, 7993-7997. (c) El-Kabbani, O.; Chang, C.-H.; Tiede, D.; Norris, J.; Schiffer, M. *Biochemistry* **1991**, *30*, 5361-5369.

(2) (a) Parson, W. W.; Warshel, A. *J. Am. Chem. Soc.* **1987**, *109*, 6152-6163. (b) Won, Y.; Friesner, R. A. *J. Phys. Chem.* **1988**, *92*, 2214-2219. (c) Eccles, J.; Honig, B.; Schulten, K. *Biophys. J.* **1988**, *53*, 137-144. (d) Rosenbach-Belkin, V.; Fisher, J. R. E.; Scherz, A. *J. Am. Chem. Soc.* **1991**, *113*, 676-678. (e) Friesner, R. A.; Won, Y. *Biochim. Biophys. Acta* **1989**, *977*, 99-102 and references therein.

(3) (a) Scherer, P. O. J.; Fischer, S. F. *Chem. Phys.* **1989**, *131*, 115-127. (b) Thompson, M. A.; Zerner, M.; Fajer, J. *J. Phys. Chem.* **1991**, *95*, 5693-5700.

(4) (a) *The photosynthetic bacterial reaction center. Structure and Dynamics*; Breton, J., Vermeglio, A., Eds.; Plenum: New York, 1988. (b) Kirmaier, C.; Holten, D. *Photosynth. Res.* **1987**, *13*, 165-180. (c) Boxer, S. G.; Goldstein, R. A.; Lockhart, D. J.; Middendorf, T. R.; Takiff, L. *J. Phys. Chem.* **1989**, *93*, 8280-8294.

(5) (a) Chandra, A. C.; Lim, E. C. *J. Phys. Chem.* **1968**, *48*, 2589-2595. (b) Murrell, J. N.; Tanaka, J. *Mol. Phys.* **1964**, *4*, 363-380. (c) Azumi, T.; McGlynn, S. P. *J. Chem. Phys.* **1965**, *42*, 1675-1680. (d) Vala, M. T., Jr.; Hillier, I. H.; Rice, S. A.; Jortner, J. *J. Chem. Phys.* **1966**, *44*, 23-35. (e) Warshel, A.; Huler, E. *Chem. Phys.* **1974**, *6*, 463-468.

(6) (a) Cram, D. J.; Allinger, N. L.; Steinberg, H. *J. Am. Chem. Soc.* **1954**, *76*, 6132-6141. (b) Koutecky, J.; Paldus, J. *Collect. Czech. Chem. Commun.* **1962**, *27*, 599-617. (c) Koutecky, J.; Paldus, J. *Tetrahedron* **1963**, *19*, 201-221. (d) Ron, A.; Schnepp, O. *J. Chem. Phys.* **1962**, *37*, 2540-2546. (e) Ron, A.; Schnepp, O. *J. Chem. Phys.* **1966**, *44*, 19-22.

(7) Girolami, G. S.; Milam, S. N.; Suslick, K. S. *J. Am. Chem. Soc.* **1988**, *110*, 2011-2012.

(8) (a) Buchler, J. W.; De Cian, A.; Fischer, J.; Kihn-Botulinski, M.; Paulus, H.; Weiss, R. *J. Am. Chem. Soc.* **1986**, *108*, 3652-3659. (b) Buchler, J. W.; De Cian, A.; Fischer, J.; Hammerschmitt, P.; Loffler, J.; Scharbert, B.; Weiss, R. *Chem. Ber.* **1989**, *122*, 2219-2228.

(9) Buchler, J. W.; De Cian, A.; Fischer, J.; Hammerschmitt, P.; Weiss, R. *Chem. Ber.* **1991**, *124*, 1051-1058.

(10) Cho, S.-H.; Kim, H.-J.; Kim, H.; Lee, W.; Gorlin, P. A.; Girolami, G. S.; Suslick, K. S. *Inorg. Chem.* **1991**, *30*, 2652-2656.

(11) (a) Buchler, J. W.; Scharbert, B. *J. Am. Chem. Soc.* **1988**, *110*, 4272-4276. (b) Buchler, J. W.; Elasser, K.; Kihn-Butulinski, M.; Scharbert, B. *Angew. Chem., Int. Ed. Engl.* **1986**, *25*, 286-287. (c) Buchler, J. W.; Hammerschmitt, P.; Kaufeld, I.; Loffler, J. *Chem. Ber.* In press. (d) Markovitsi, D.; Tran-Thi, T.-H.; Even, R.; Simon, J. *Chem. Phys. Lett.* **1987**, *137*, 107-112. (e) Buchler, J. W.; Hammerschmitt, P.; Kaufeld, I.; Loffler, J. *Chem. Ber.* **1991**, *124*, 2151-2159.

(12) (a) Girolami, G. S.; Milam, S. N.; Suslick, K. S. *Inorg. Chem.* **1987**, *26*, 343-344. (b) Milam, S. N. Doctoral Thesis, University of Illinois at Urbana-Champaign, 1989.

(13) Yan, X.; Holten, D. *J. Phys. Chem.* **1988**, *92*, 409-414.

(14) Bilsel, O.; Rodriguez, J.; Holten, D. *J. Phys. Chem.* **1990**, *94*, 3508-3512.

0002-7863/92/1514-6528$03.00/0

(≥3000 cm^{-1}) shifted from this new low-energy absorption,[15,16] and prominent NIR features in the spectra of the (π,π^*) excited states[16] and the π-radical cations generated by oxidation of the sandwich complexes.[7-12,17,18] We have argued that the new red region absorption and fluorescence of the sandwich complexes cannot be explained by exciton coupling. Rather, these properties must be associated with excited states that have significant contributions from CT configurations and, thus, with transitions involving delocalized molecular orbitals of a supermolecule.[14-16] The NIR, ESR, and Raman spectra of the electron deficient sandwich complexes[11e,17,18] and the NIR band of the oxidized ZnOEP dimer[19] have been successfully interpreted using a supermolecule MO approach. However, additional studies of the electronic states and optical properties of the sandwich complexes are needed to help elucidate further the factors that contribute to the electronic structure of these complexes, the special pair in the photosynthetic reaction center, and strongly interacting π systems in general.

In this paper, we report the ground state absorption, fluorescence, and phosphorescence spectra and the time-resolved (π,π^*) excited state absorption behavior of the Th^{IV} porphyrin sandwich complexes $Th(TPP)_2$, $Th(OEP)_2$, and Th(OEP)(TPP).[20a] We also present in detail a model that accounts for all of the optical characteristics of the sandwich complexes and extends our understanding of strongly-coupled porphyrins.

Experimental Section

The symmetric complexes $Th(TPP)_2$ and $Th(OEP)_2$ were synthesized and characterized as described previously.[7,12] The asymmetric compound Th(OEP)(TPP) was synthesized in a similar manner.[20b] Samples used for emission studies were further purified by column chromatography on basic alumina (Brockman Activity I, predried under vacuum at ~100 °C for 30 min) with toluene as the eluent.

Ground-state absorption spectra were recorded on a Perkin-Elmer Lambda 3B spectrophotometer. The samples used for emission studies had an absorbance ≤1.0 at the excitation wavelength (normally in the Soret region). Fluorescence measurements utilized a Spex Fluorolog II spectrofluorometer equipped with an R928 photomultiplier tube and photon counting electronics. Phosphorescence spectra were recorded using an RCA C30956E Si avalanche photodiode and lock-in detection. Detection bandwidths of ~10 nm for fluorescence and ~15 nm for phosphorescence were used.

Time-resolved absorption spectra in the sub-nanosecond regime were recorded on instruments described elsewhere.[21] Samples having a concentration of ~10 μM in 2 mm path length cells were excited with a 100 fs, 582 nm, 150 μJ pulse and probed as a function of delay times with a broad band (385–965 nm) pulse of comparable duration. Microsecond and longer-time transient absorption measurements utilized an apparatus employing 10 ns, 532 nm, 10 mJ excitation pulses[22] and ~1 μM samples in 1 cm path length cells that were deoxygenated by repeated freeze–pump–thaw cycles on a high-vacuum line. Studies at low temperature employed an Oxford Instruments cryostat system.

Results

Ground Electronic State Absorption Spectra. Ground-state absorption spectra of the three Th^{IV} bis(porphyrin) sandwich complexes at 295 K are shown in Figure 1. The spectra of

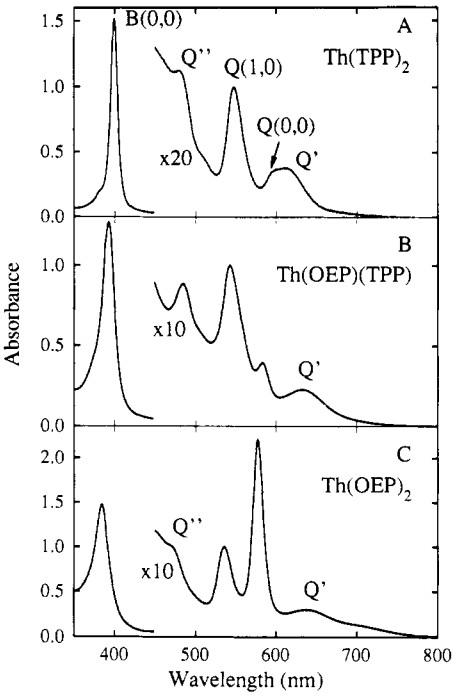

Figure 1. Ground-state absorption spectra of the three Th^{IV} sandwich complexes in toluene at 295 K: (A) $Th(TPP)_2$, (B) Th(OEP)(TPP), (C) $Th(OEP)_2$. The 450–800-nm region has been multiplied by the indicated factor and the spectra have been normalized to 1.0 at the Q(1,0) absorption maximum.

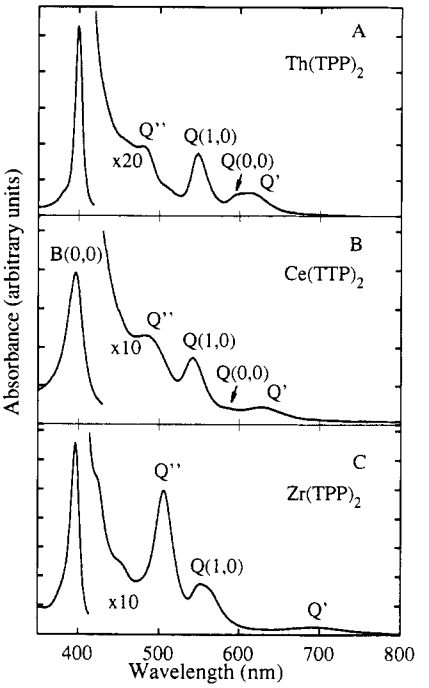

Figure 2. Comparison of the ground-state absorption spectra of (A) $Th(TPP)_2$, (B) $Ce(TTP)_2$, and (C) $Zr(TPP)_2$. All three spectra were recorded in toluene at 295 K. The ~420–800-nm region has been multiplied by the indicated factor. It is of interest to note that the ionic radii of the +4 metals are 1.02 Å for Th^{IV}, 0.92 Å for Ce^{IV}, and 0.79 Å for Zr^{IV}.

$Th(OEP)_2$, $Th(TPP)_2$, and Th(OEP)(TPP) are similar to those found for the three analogous Ce^{IV} sandwich complexes[8,11,14] and for the corresponding symmetric U^{IV}, Zr^{IV}, and Hf^{IV} complexes[9,10,12] (see Figure 2). The spectra of $Th(OEP)_2$ and $Th(TPP)_2$ exhibit the following characteristics: (i) Bands are present between 530 and 590 nm that have essentially the same position, intensity, and macrocycle dependence exhibited by analogous mono(porphyrin) complexes.[23,24] Specifically, the Q(0,0) band of $Th(OEP)_2$

(15) Bilsel, O.; Rodriguez, J.; Holten, D.; Girolami, G. S.; Milam, S. N.; Suslick, K. S. *J. Am. Chem. Soc.* **1990**, *112*, 4075–4077.
(16) Bilsel, O.; Buchler, J. W.; Hammerschmitt, P.; Rodriguez, J.; Holten, D. *Chem. Phys. Lett.* **1991**, *182*, 415–421.
(17) (a) Donohoe, R. J.; Duchowski, J. K.; Bocian, D. F. *J. Am. Chem. Soc.* **1988**, *110*, 6119–6124. (b) Duchowski, J. K.; Bocian, D. F. *J. Am. Chem. Soc.* **1990**, *112*, 3312–3318. (c) Perng, J.-H.; Duchowski, J. K.; Bocian, D. F. *J. Phys. Chem.* **1990**, *94*, 6684–6691.
(18) (a) Duchowski, J. K.; Bocian, D. F. *J. Am. Chem. Soc.* **1990**, *29*, 4159. (b) Duchowski, J. K.; Bocian, D. F. *Inorg. Chem.* **1990**, *29*, 4158–4160. (c) Perng, J.-H.; Duchowski, J. K.; Bocian, D. F. *J. Phys. Chem.* **1991**, *95*, 1319–1323.
(19) Fuhrhop, J. H.; Wasser, P.; Reisner, D.; Mauzerall, D. *J. Am. Chem. Soc.* **1972**, *94*, 7996–8001.
(20) (a) OEP is 2,3,7,8,12,13,17,18-octaethylporphyrinate(2−); TPP is 5,10,15,20-tetraphenylporphyrinate(2−); TTP is 5,10,15,20-tetratolylporphyrinate(2−). (b) Girolami, G. S.; Gorlin, P. A.; Suslick, K. S. Unpublished work.
(21) (a) Kirmaier, C.; Holten, D. *Biochemistry* **1991**, *30*, 609–613. (b) Kim, D. H.; Kirmaier, C.; Holten, D. *Chem. Phys.* **1983**, *75*, 305–322.
(22) Tait, C. D.; Holten, D.; Barley, M. H.; Dolphin, D.; James, B. R. *J. Am. Chem. Soc.* **1985**, *107*, 1930–1934.

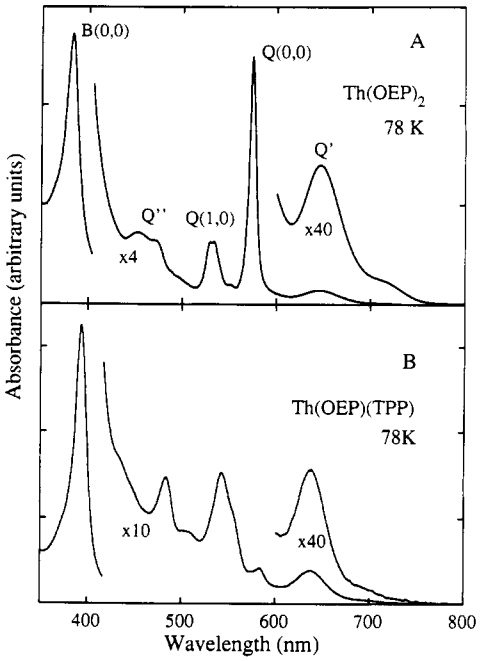

Figure 3. Low-temperature ground-state absorption spectra of (A) Th(OEP)$_2$ and (B) Th(OEP)(TPP) recorded at 78 K in a 3-methylpentane glass.

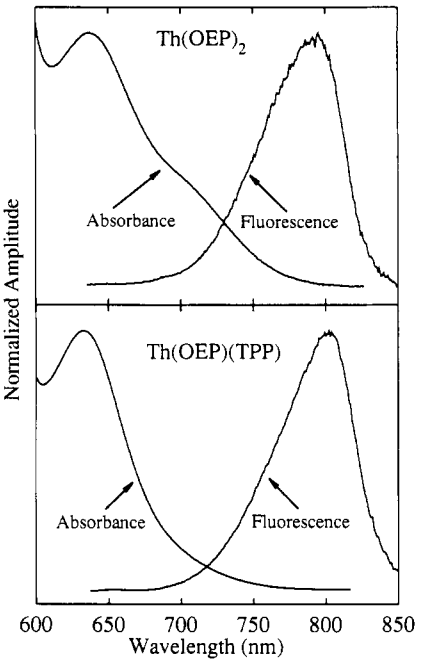

Figure 4. Normalized absorption and fluorescence spectra of Th(OEP)$_2$ (top panel) and Th(OEP)(TPP) (bottom panel) recorded in nondegassed toluene at 295 K. The spectra have been corrected for the detection system response. Excitation spectra confirmed that the fluorescence is due to the indicated complex.

at 575 nm is stronger than the 545-nm Q(1,0) band, whereas, for Th(TPP)$_2$ the Q(0,0) band near 590 nm is barely discernable and much weaker than the 550-nm Q(1,0) band. (ii) The intense near-UV Soret, or B(0,0), band is blue shifted from the position in the corresponding mono(porphyrin) complexes of the same macrocycle. (iii) A broad weak feature which we refer to as the Q′ band[15,16] is observed to the red (600–650 nm) of the monoporphyrin-like Q bands. (iv) A band denoted Q″ is observed to the blue (465–505 nm) of the monoporphyrin-like Q bands. Additionally, there is evidence that additional weak features underly the broad absorption between the Soret and Q bands. The Q′ and Q″ bands are also present in the spectrum of the nonsymmetric sandwich complex, Th(OEP)(TPP). However, for this complex, Ce(OEP)(TTP),[14] and Ce(OEP)(TPP)[8b] the Q(0,0) band is much weaker than expected from the sum of Q bands of typical metallo-OEP and -TPP complexes (Figure 1).

We believe the new Q′ and Q″ absorptions to be highly characteristic of strongly-coupled porphyrins. The features are observed for all the "neutral" bis(porphyrin) sandwich complexes (those containing a +4 metal ion and hence filled ring π-HOMOs)[7-14] but not for the corresponding mono(porphyrin) complexes[23,24] or bis(porphyrin) complexes with larger macrocycle spacings.[25,26] Variations in these features also correlate with the ionic radius of the metal ion and thus the distance between the two rings. First, the Q′ absorption maximum shifts to the red as the ionic radius of the metal ion decreases (Figure 2); the Q′ band lies at 615 nm for Th(TPP)$_2$, 630 nm for Ce(TPP)$_2$, and ~700 nm for Hf(TPP)$_2$ and Zr(TPP)$_2$ (Zr and Hf have very similar ionic radii). The metal–metal bonded porphyrin dimers also exhibit red-region absorptions that may be, in part, of Q′ origin.[27] Second, the Q″ band red shifts and gains intensity as the separation between the macrocycles decreases (Figure 2).

Several minor changes are observed in the ground-state absorption spectra of the Th^{IV} complexes at 78 K (Figure 3). For Th(OEP)$_2$, the most prominent change is the emergence of two distinct bands in the Q″ region in addition to a general sharpening of the spectrum. The Q′ band remains considerably broader than the other features in the spectrum, although better resolution of the shoulder near 710 nm is observed. This shoulder may correspond to the Q′ transition origin[15] and is not resolved in the TPP-substituted sandwich complexes (Figures 1 and 2). The spectrum of Th(OEP)(TPP) at 78 K is similar to that of Ce(OEP)(TPP)[14] in that several features to higher energy than the Q(0,0) band are distinguishable that were unresolved at 295 K. The Q′ absorption again remains unusually broad at 78 K.

Fluorescence and Phosphorescence. Th(OEP)$_2$ was the first sandwich complex for which Q′ fluorescence was observed.[15] For this complex and Th(OEP)(TPP) (Figure 4) and Th(TPP)$_2$ (not shown), the fluorescence is found ~3000 cm^{-1} to the red of the Q′ absorption maximum even in the nonpolar solvent toluene. No fluorescence is observed in the 580–650-nm region where mono(porphyrin) complexes typically fluoresce (just to the red of the Q(0,0) absorption[23,24]). Similar fluorescence behavior has also been observed for the Zr and Hf sandwich complexes, except the latter exhibit a larger separation between the Q′ absorption and fluorescence maxima.[16,28]

The emission spectra of all three thorium bis(porphyrin) sandwich complexes in degassed toluene solutions as a function of temperature are shown in Figure 5A–C. The phosphorescence observed between 900 and 1000 nm is spectrally broad and has a maximum significantly to the red of the phosphorescence of typical OEP and TPP mono(porphyrin) complexes (700–800 nm).[23,24] Near room temperature, a shoulder is found ~2000 cm^{-1}

(23) Martano, L. A.; Wong, C.-P.; Horrocks, W. D., Jr.; Goncalves, A. M. P. *J. Phys. Chem.* **1976**, *80*, 2389–2393.
(24) Gouterman, M. In *The Porphyrins*; Dolphin, D., Ed.; Academic Press: New York, 1979; Vol. III, pp 1–165.
(25) (a) Gouterman, M.; Holten, D.; Lieberman, E. *Chem. Phys.* **1977**, *25*, 139–153. (b) Hunter, C. A.; Sanders, J. K. M.; Stone, A. J. *Chem. Phys.* **1989**, *133*, 395–404. (c) Won, Y.; Friesner, R. A.; Johnson, M. R.; Sessler, J. L. *Photosynth. Res.* **1989**, *22*, 201–210. (d) Erikkson, S.; Källebring, B.; Larsson, S.; Martensson, J.; Wennerström, O. *Chem. Phys.* **1990**, *165*, 165–177.
(26) (a) Chang, C. K. *J. Heterocycl. Chem.* **1977**, *14*, 1285–1288. (b) Collman, J. P.; Anson, F. C.; Barnes, C. E.; Bencosme, C. S.; Geiger, T.; Evitt, E. R.; Kreh, R. P.; Meier, K.; Pettman, R. B. *J. Am. Chem. Soc.* **1983**, *105*, 2694–2699. (c) Bocian, D. F.; Findsen, E. W.; Horrman, J. A., Jr.; Schick, G. A.; English, D. R.; Hendrickson, N.; Suslick, K. S. *Inorg. Chem.* **1984**, *23*, 800–807. (d) Osuka, A.; Maruyama, K. *J. Am. Chem. Soc.* **1988**, *110*, 4454–4456.
(27) (a) Collman, J. P.; Barnes, C. E.; Collins, T. J.; Brothers, P. J.; Gallucci, J.; Ibers, J. A. *J. Am. Chem. Soc.* **1981**, *103*, 7030–7032. (b) Collman, J. P.; Barnes, C. E.; Swepston, P. N.; Ibers, J. A. *J. Am. Chem. Soc.* **1984**, *106*, 3500–3510.
(28) (a) Bilsel, O.; Girolami, G. S.; Buchler, J. W.; Gorlin, P. A.; Hammerschmitt, P.; Rodriguez, J.; Suslick, K. S.; Holten, D. Manuscript in preparation on the optical and photophysical properties of Zr(OEP)$_2$ and Hf(OEP)$_2$. (b) Bilsel, O. Ph.D. Thesis, Washington University, August 1991.

Table I. Excited-State Decay Kinetics[a]

complex	temp (K)	$^1Q'(\pi,\pi^*)$ (ps)	$^3T'(\pi,\pi^*)$ 1-exp (μs)	$^3T'(\pi,\pi^*)$ 2-exp (μs)	$^3T'(\pi,\pi^*)$ $\chi_{1\text{-exp}}^2/\chi_{2\text{-exp}}^2$
$Th(OEP)_2$	295	13 ± 2	8.9 ± 0.4	3.4 ± 0.5/9.4 ± 0.1	1.09
	78			95 ± 0.1/450 ± 30	7.4[b]
Th(OEP)(TPP)	295	27 ± 3	36.2 ± 0.3	26.6 ± 3.0/40.4 ± 2.0	1.04
	77		372 ± 20	188 ± 20/453 ± 15	1.33
$Th(TPP)_2$	295	~60	39.4 ± 0.5		1.01

[a] Data at 295 K obtained using degassed toluene solutions; data at low temperatures obtained using 3-methylpentane glasses. The $^3T'(\pi,\pi^*)$ lifetimes were analyzed using single- and dual-exponential functions and the ratio of the χ^2 values is given in the last column. [b] The χ^2 ratio for data acquired at the Soret maximum. The ratio is larger when global analysis of the data across the Soret band is used.

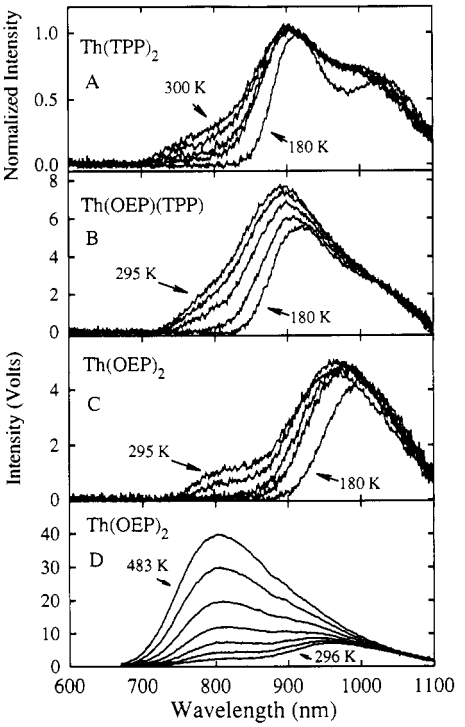

Figure 5. Corrected phosphorescence spectra of the three Th^{IV} porphyrin sandwich complexes in degassed toluene solution. (A) Normalized phosphorescence spectra of $Th(TPP)_2$ recorded at 180 K (indicated by arrow) followed by spectra at 240, 270, 285, and 300 K with increasing intensity in the 765-nm region. (B) Phosphorescence spectra of Th(OEP)(TPP) recorded (in ascending order near the 800-nm region) at 180, 240, 270, 285, and 295 K. (C) Phosphorescence spectra of $Th(OEP)_2$ shown, similarly, at 180, 240, 270, 285, and 295 K. Excitation spectra acquired detecting at the phosphorescence maximum and the high-energy shoulder (at 295 or 300 K) were similar to each other and also to the corresponding absorption spectrum. (D) Phosphorescence spectra of $Th(OEP)_2$ in silicone oil given as a function of temperature from 295 to 483 K. Temperature readings are correct to ±0.1 K for panels A–C and ±1 K for panel D.

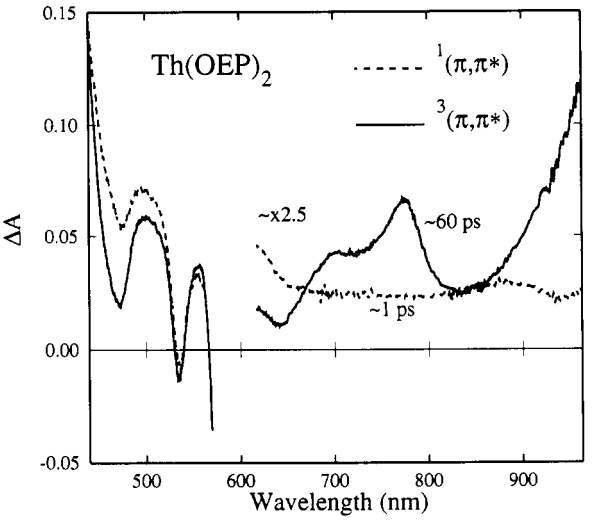

Figure 6. Transient absorption spectra of $Th(OEP)_2$ in toluene at 295 K recorded ~1 ps (dashed lines) and ~60 ps (solid lines) after excitation with a 582-nm, 150-fs, ~100-μJ pulse. The spectrum between 600 and 965 nm has been multiplied by 2.5.

to higher energy for each complex. Two observations indicate that the high-energy shoulder is mainly delayed fluorescence: (i) For a nondegassed $Th(OEP)_2$ solution at 295 K, not only is the overall emission intensity significantly reduced relative to a deoxygenated sample but the ~790 nm emission is also larger by a factor of 3.5 upon normalization at the 960-nm phosphorescence peak. (This result indicates that even in nondegassed solutions at 295 K about 30% of the fluorescence yield of $\sim 10^{-5}$ for $Th(OEP)_2$[15] represents delayed fluorescence.) (ii) The intensity of the emission between 750 and 800 nm decreases systematically as the temperature is lowered, being practically absent at 180 K (Figure 5A–C). Additionally, the emission is dominated by the higher energy (delayed fluorescence) feature when the temperature is raised to 483 K for $Th(OEP)_2$ (Figure 5D) and Th(OEP)(TPP) (not shown). The underlying effects of heating and cooling appear to be complex, however, as evidenced by the fact that satisfactory global fits to the data of Figure 5D using only two Gaussian functions are successful only if the positions of these functions are allowed to vary with temperature. Nonetheless, the temperature dependence of the delayed fluorescence yields an estimate for the activation energy of ~ 1700 cm^{-1}.

Excited-State Absorption and Kinetics. Figure 6 (dashed line) shows the visible/NIR excited-state absorption spectrum of $Th(OEP)_2$ observed ~1 ps after excitation with a 100-fs 582-nm flash. Since this spectrum is representative of what is observed immediately following the flash, we assign it to the fluorescent $^1Q'(\pi,\pi^*)$ state. For comparison, the $^1(\pi,\pi^*)$ states of monoporphyrins show a similarly featureless absorption broken by bleaching of the ground-state absorption bands.[29] The 1-ps spectrum evolves with a time constant of 13 ± 2 ps[30a] into the spectrum shown at ~60 ps (solid line). Similar behavior is observed for Th(OEP)(TPP) and $Th(TPP)_2$, except that these complexes exhibit somewhat longer decay times of the $^1Q'(\pi,\pi^*)$ excited state (Table I).

No appreciable changes occur in the transient spectrum of $Th(OEP)_2$ after 60 ps up to the 4-ns time limit of the femtosecond spectrometer. This observation suggests that the 60-ps spectrum is due to the lowest $^3(\pi,\pi^*)$ state. This interpretation is supported by the prominent absorption near 775 nm for $Th(OEP)_2$ and a smaller absorption ~ 1500 cm^{-1} to the blue. The NIR $^3(\pi,\pi^*)$ spectra of monomeric OEP and TPP complexes generally consist of two such bands built on a featureless background absorption with the longer-wavelength feature having, as is observed here, an intensity about 30% that of the Q(1,0) ground-state absorption band (i.e., log $\epsilon \sim 3.7$).[29,30d]

(29) Rodriguez, J.; Kirmaier, C.; Holten, D. *J. Am. Chem. Soc.* **1989**, *111*, 6500–6506.

(30) (a) For $Th(OEP)_2$ the time constant for decay of $^1Q'(\pi,\pi^*)$ varies from 10 to 15 ps across the 450–500-nm region. As has been found and discussed for other metalloporphyrins,[30b,c] including the Ce porphyrin sandwich complexes,[14] this may be due to incomplete vibrational equilibration within the electronic excited state. (b) Rodriguez, J.; Holten, D. *J. Chem. Phys.* **1989**, *91*, 3525–3531. (c) Rodriguez, J.; Kirmaier, C.; Holten, D. *J. Chem. Phys.* **1991**, *94*, 6020–6029. (d) Well-resolved NIR $^3(\pi,\pi^*)$ spectra similar to Figure 6 for $Th(OEP)_2$ were not obtainable for the other complexes due to their lower solubility.

In addition to the two monoporphyrin-like $^3(\pi,\pi^*)$ features, $Th(OEP)_2$ shows a much more intense NIR excited state absorption with a peak slightly past 1000 nm (Figure 6). A similarly intense NIR $^3(\pi,\pi^*)$ feature is observed for $Zr(TPP)_2$ and $Hf(TPP)_2$,[16] and for the corresponding OEP compounds.[28] However, for the Zr and Hf complexes, the two monoporphyrin-like features between 700 and 850 nm are not as clearly resolved due, most likely, to spectral overlap with the more intense $^3(\pi,\pi^*)$ band of the sandwich complexes which moves to higher energy as the ionic radius of the metal decreases. We estimate the quantum yield of the $^3(\pi,\pi^*)$ state to be at least 90% in the Th sandwich complexes, based on the minimal decay of bleaching in the ground-state bands as $^1Q'(\pi,\pi^*)$ evolves to $^3(\pi,\pi^*)$ (e.g., see Figure 6).[15]

Decay of the $^3(\pi,\pi^*)$ state occurs on the microsecond time scale, as determined by recovery of the bleaching in the Soret band following a 10-ns 532-nm flash. Analysis of the kinetics by local and global nonlinear least-squares methods[31] suggests that although the decay of the $^3(\pi,\pi^*)$ state of $Th(TPP)_2$ in degassed toluene solution at 295 K can be fit well by a monoexponential function ($\tau = 39.4 \pm 0.5$ μs), it is questionable whether the same holds true for $Th(OEP)_2$ and Th(OEP)(TPP). This is especially true at 77 K, where the lifetimes are also significantly longer than at 295 K (Table I).

Discussion

Comparison with Weakly-Coupled Systems. The sandwich complexes have characteristic optical properties that include (i) monomer-like ground-state absorption features, (ii) a new Q″ absorption band at higher energy and a Q′ absorption band at lower energy than the monomer-like Q bands, (iii) a broad weak Q′ fluorescence band substantially red shifted from the Q′ absorption maximum, (iv) prominent excited-state absorption in the NIR having no counterpart in the spectra of mono(porphyrin) complexes, and (v) a phosphorescence band significantly red shifted from those of typical mono(porphyrin) complexes.

Exciton coupling using the dipole–dipole approximation can be used to rationalize the blue shift of the *intense* Soret band and the presence, in the symmetric sandwich complexes, of *weak* Q bands having positions and intensities similar to those of mono(porphyrin) complexes. This approach has likewise provided a satisfactory explanation for the blue-shifted Soret and relatively unperturbed Q bands for porphyrin dimers having larger spacings between the macrocycles (e.g. μ-oxo complexes).[25,26] However, exciton coupling of the weak Q transitions of the subunits cannot explain several key spectral characteristics of the sandwich complexes.[14-16] For example, exciton theory cannot account for new Q′ absorption ~3000 cm^{-1} lower than the mono(porphyrin)-like Q bands and the significantly perturbed Q bands of the asymmetric complexes Th(OEP)(TPP) (Figure 1), Ce(OEP)(TTP),[14] and Ce(OEP)(TPP).[8b] Furthermore, although simple exciton theory can account for some small absorption between the Soret and Q bands, it cannot account for the intensity of the Q″ absorption in transition metal sandwich complexes such as $Zr(TPP)_2$ (Figure 2).[16]

Simple exciton theory neglects overlap of the orbitals of the subunits. The new optical features in the ground-state absorption spectra of the sandwich complexes are not observed in mono(porphyrin) complexes or dimers with larger ring spacings. In addition, these features vary systematically with the ionic radius of the metal ion (Figure 2). Therefore, the new optical features derive from orbital overlap between the π systems of the subunits and must involve transitions among orbitals that are delocalized over both porphyrins of the complex.[14-16] Similarly, the NIR band of electron-deficient sandwich complexes[11e,17,18] and of the ZnOEP dimer cation[19] has been assigned by using a delocalized MO approach. In other words, a proper description of the electronic states of the sandwich complexes requires consideration of the wave functions of a supermolecule.

General Approaches for Characterizing the States of Strongly-Coupled Systems. Analysis of strongly-coupled chromophores such as aromatic hydrocarbon excimers,[5] paracyclophanes,[6] and the reaction center special pair[2,3] have proceeded in two general directions. One approach is to start with locally-excited configurations (A*B and AB*) of two chromophores (designated A and B) as is done in simple exciton theory. Additionally, due to the non-negligible overlap between the two macrocycles, charge transfer (CT) or ionic configurations (A^+B^- and A^-B^+) must be considered. In the case where the two chromophores are identical, properly symmetrized wave functions would consist of linear combinations of the respective parent configurations, $EX^{\pm} = (A^*B \pm AB^*)/2^{1/2}$ and $CR^{\pm} = (A^+B^- \pm A^-B^+)/2^{1/2}$. Consistent with the literature on a variety of systems[5b-e,32,34] and our previous work on the sandwich complexes,[15,16] we refer to the latter as charge-resonance (CR) configurations. If the two chromophores A and B are identical (and in the absence of solvent effects), there is no net transfer of charge from one ring to the other. For non-identical chromophores, a configuration with substantial, but unequal, contributions of the two opposing CT configurations also can be described as having CR parentage. The excited states are then obtained from mixing of the CR and EX configurations under the Hamiltonian of the coupled system.

The second general approach involves construction of supermolecule MOs from linear combinations of the subunit MOs. One then obtains excited configurations in the traditional manner by considering electron promotions from the occupied to unoccupied MOs. Configuration interaction among the basis configurations is important in properly describing the excited states of the system (see below).[5a,6b] The supermolecule MO and EX/CR wave functions are related by a basis transformation.

A Model for the Electronic States of the Porphyrin Sandwich Complexes. In a recent study of $Zr(TPP)_2$ and $Hf(TPP)_2$, we outlined a simple MO picture and its relationship to the EX/CR description; this model rationalizes the key experimental observations on the neutral sandwich complexes[16] and is elaborated in detail here. Supermolecule MO approaches have been used previously to describe the optical properties of the oxidized sandwich complexes,[17] bacteriochlorin dimers,[34a] the reaction center special pair,[3] aromatic excimers,[5a] and paracyclophanes.[6b] Within the supermolecule MO approach, we express the MOs of the sandwich complexes in terms of the $a_{1u}(\pi)$ and $a_{2u}(\pi)$ HOMOs and $e_g(\pi^*)$ LUMOs of the four-orbital model[24,35] that has been so successful in describing the electronic states of mono(porphyrin) complexes. For simplicity, the common D_{4h} symmetry notation will be used for the mono(porphyrin) orbitals although the sandwich complexes have approximate D_{4d} symmetry since the two cofacial macrocycles are rotated about 40° with respect to one another.[7-10] Accordingly, the bonding (on the left) and antibonding (on the right) MOs of this eight-orbital model of the bis(porphyrin) are given as follows[36] (Figure 7):

$$\begin{aligned} b_1 &= (a_{1u}^A + a_{1u}^B)/2^{1/2} & a_2 &= (a_{1u}^A - a_{1u}^B)/2^{1/2} \\ b_2 &= (a_{2u}^A + a_{2u}^B)/2^{1/2} & a_1 &= (a_{2u}^A - a_{2u}^B)/2^{1/2} \\ e_{3xz} &= (e_{gx}^A + e_{gx}^B)/2^{1/2} & e_{1x} &= (e_{gx}^A - e_{gx}^B)/2^{1/2} \\ e_{3yz} &= (e_{gy}^A + e_{gy}^B)/2^{1/2} & e_{1y} &= (e_{gy}^A - e_{gy}^B)/2^{1/2} \end{aligned} \quad (1)$$

(31) (a) Marquardt, D. W. *J. Soc. Ind. Appl. Math.* **1963**, *11*, 431-441. (b) Knutson, J. R.; Beechem, J. M.; Brand, L. *Chem. Phys. Lett.* **1983**, *102*, 501-507.

(32) McDowell, L. M.; Kirmaier, C.; Holten, D. *Biochim. Biophys. Acta* **1990**, *1020*, 239-246.

(33) Ohno, O.; Ishikawa, N.; Matsuzawa, T.; Kobayashi, H. *J. Phys. Chem.* **1989**, *93*, 1713-1718.

(34) (a) Thompson, M. A.; Zerner, M. C.; Fajer, J. *J. Phys. Chem.* **1990**, *94*, 3820-3828. (b) Petke, J. D.; Maggiora, G. M. *J. Chem. Phys.* **1986**, *84*, 1640-1652.

(35) (a) Gouterman, M. *J. Chem. Phys.* **1959**, *30*, 1139-1161. (b) Gouterman, M. *J. Mol. Spectrosc.* **1961**, *6*, 138-163. (c) Gouterman, M.; Wagniere, G. H.; Snyder, L. C. *J. Mol. Spectrosc.* **1963**, *11*, 108-127.

(36) Since the overlap integrals $\langle a_{1u}^A|a_{1u}^B\rangle$, $\langle a_{2u}^A|a_{2u}^B\rangle$, and $\langle e_g^A|e_g^B\rangle$ are likely to be comparatively small ($S < 0.1$[33,37]), they are omitted in normalization of the MOs. The phases of the supermolecule MOs have been derived using the convention that the positive lobes of the orbitals on equivalent atoms of the subunits point in the same direction and that the overlap integrals are all positive.[37]

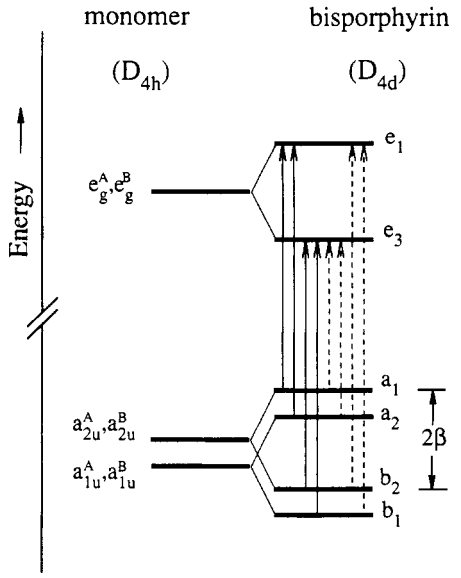

Figure 7. Schematic molecular orbital diagram of the supermolecule molecular orbitals (right side) formed from linear combinations of the 4-orbital MOs (left side) of the constituent mono(porphyrin) complexes. The solid arrows are used to denote the dipole-allowed E_1 one-electron configurations and the dashed arrows are used for the E_3 dipole-forbidden one-electron configurations. The energy spacings (2β) between the bonding/antibonding pairs of MOs are not drawn to scale, as indicated by the break in the energy axis.

The energy splittings between the bonding and antibonding MOs are *twice* the respective intermolecular resonance integrals: $\beta_1 = \langle a_{1u}{}^A|H_{eff}|a_{1u}{}^B\rangle$, $\beta_2 = \langle a_{2u}{}^A|H_{eff}|a_{2u}{}^B\rangle$, and $\beta_e = \langle e_g{}^A|H_{eff}|e_g{}^B\rangle$, where H_{eff} is the effective one-electron Hamiltonian and $H = H_{eff} + \sum e^2/r_{ij}$. Although the three β integrals are not exactly equal,[37] it is convenient to choose $\beta_1 \sim \beta_2 \sim \beta_e$. Hence, the splittings between the bonding/antibonding MO pairs are equal in Figure 7.

In describing the electronic states of the sandwich complexes we use the π-electron approximation and consider only the singly-excited configurations involving the bis(porphyrin) MOs listed above and in Figure 7. There will be 16 possible excited configurations, the irreducible representation of which will be either E_1 or E_3 under D_{4d} symmetry:

E_{1x}: (a_1e_{1x}), (a_2e_{1y}), (b_2e_{3xz}), (b_1e_{3yz})

E_{1y}: (a_1e_{1y}), (a_2e_{1x}), (b_2e_{3yz}), (b_1e_{3xz})

E_{3xz}: (a_1e_{3xz}), (a_2e_{3yz}), (b_2e_{1x}), (b_1e_{1y})

E_{3yz}: (a_1e_{3yz}), (a_2e_{3xz}), (b_2e_{1y}), (b_1e_{1x})

where, for example,

$$^1(a_1e_{1x}) = [|a_1a_2\bar{a}_2b_1\bar{b}_1b_2\bar{b}_2\bar{e}_{1x}| + |e_{1x}a_2\bar{a}_2b_1\bar{b}_1b_2\bar{b}_2\bar{a}_1|]/2^{1/2} \quad (2a)$$

$$^3(a_1e_{1x}) = [|a_1a_2\bar{a}_2b_1\bar{b}_1b_2\bar{b}_2\bar{e}_{1x}| - |e_{1x}a_2\bar{a}_2b_1\bar{b}_1b_2\bar{b}_2\bar{a}_1|]/2^{1/2} \quad (2b)$$

and $|abcd...|$ denotes a properly normalized Slater determinant. Since the LUMOs of the subunits are doubly degenerate, the singly-excited electronic configurations of the supermolecule are doubly degenerate. Thus, in deducing the singlet excited states the problem reduces to consideration of four dipole-allowed configurations having E_1 symmetry (e.g. the E_{1y} configurations) and four E_3 configurations (e.g. the E_{3yz} configurations) which are dipole forbidden in precise D_{4d} symmetry. We will therefore follow the mono(porphyrin) four-orbital model approach[35] and show explicitly only the *y*- and *yz*-polarized bis(porphyrin) configurations, less the polarization subscripts.

Singlet Electronic States Derived from the Dipole-Allowed E_1 Configurations: The Soret (B), Q″, and Q States. The fact that the position, intensity, and macrocycle dependence of the Q bands of mono(porphyrins) are retained in the symmetric sandwich complexes is extremely helpful in assessing the relative energies and mixing of the bis(porphyrin) electronic configurations. For example, it is known that the weak Q(0,0) band of monomeric TPP complexes is a consequence of the near degeneracy of the two excited configurations $^1(a_{1u}e_g)$ and $^1(a_{2u}e_g)$.[35,38]

Since the Q(0,0) band near 590 nm (Figures 1 and 2) of Th(TPP)$_2$ is also weak, an essential aspect of our model for the sandwich complexes is a near-degeneracy and considerable interaction of the four a_{1u}- and a_{2u}-derived dipole-allowed E_{1y} (or E_{1x}) configurations. Near-degeneracy of the (a_1e_1), (a_2e_1), (b_1e_3), and (b_2e_3) excited configurations arises from a combination of one- and two-electron terms. In presenting the most mathematically tractable form of the model, we follow calculations on other dimers[3a,5a,6b,33,34b] and neglect differential overlap and also adopt a cyclic polyene approximation (e.g. analogous integrals involving the a_{1u} and a_{2u} orbitals are equal).[24,28b] Appendix 1 gives the resulting interaction matrix for the singlet E_1 configurations. The eigenfunctions of this matrix are

$$B^+ = [(b_1e_3) + (b_2e_3) + (a_1e_1) + (a_2e_1)]/2 \quad (3a)$$

$$Q^+ = [(b_1e_3) - (b_2e_3) - (a_1e_1) + (a_2e_1)]/2 \quad (3b)$$

$$CR_1{}^+ = [(b_1e_3) - (a_2e_1)]/2^{1/2} \quad (3c)$$

$$CR_2{}^+ = [(b_2e_3) - (a_1e_1)]/2^{1/2} \quad (3d)$$

Expanding in terms of mono(porphyrin) MOs gives in the exciton/CR basis

$$B^+ = [a_{1u}{}^Ae_g{}^A + a_{2u}{}^Ae_g{}^A + a_{1u}{}^Be_g{}^B + a_{2u}{}^Be_g{}^B]/2 = [B^A + B^B]/2^{1/2} \quad (4a)$$

$$Q^+ = [a_{1u}{}^Ae_g{}^A - a_{2u}{}^Ae_g{}^A + a_{1u}{}^Be_g{}^B - a_{2u}{}^Be_g{}^B]/2 = [Q^A + Q^B]/2^{1/2} \quad (4b)$$

$$CR_1{}^+ = [a_{1u}{}^Ae_g{}^B + a_{1u}{}^Be_g{}^A]/2^{1/2} = [CT_1{}^{AB} + CT_1{}^{BA}]/2^{1/2} \quad (4c)$$

$$CR_2{}^+ = [a_{2u}{}^Ae_g{}^B + a_{2u}{}^Be_g{}^A]/2^{1/2} = [CT_2{}^{AB} + CT_2{}^{BA}]/2^{1/2} \quad (4d)$$

which makes more transparent the compositions of the states.[39] In eqs 4c and 4d, $CT_1{}^{AB}$, for example, corresponds to a parent CT configuration in which an electron is moved from the a_{1u} HOMO of subunit A to the e_g LUMO of ring B.

The corresponding energy eigenvalues of the E_1 singlet excited states are

$$E(B^+) = E_m + 2(a_{1u}{}^Ae_g{}^A|a_{2u}{}^Ae_g{}^A) + 4(a_{1u}{}^Ae_g{}^A|a_{2u}{}^Be_g{}^B) \quad (5a)$$

$$E(Q^+) = E_m - 2(a_{1u}{}^Ae_g{}^A|a_{2u}{}^Ae_g{}^A) \quad (5b)$$

$$E(CR_1{}^+) = \Delta\epsilon - (a_{1u}{}^Aa_{1u}{}^A|e_g{}^Be_g{}^B) \quad (5c)$$

$$E(CR_2{}^+) = \Delta\epsilon - (a_{2u}{}^Aa_{2u}{}^A|e_g{}^Be_g{}^B) \quad (5d)$$

(37) Konami, H.; Hatano, M.; Tajiri, A. *Chem. Phys. Lett.* **1990**, *166*, 605–608.

(38) The weak (0,0) band of mono(porphyrin) complexes is understood within the four-orbital model as arising from near-degeneracy of the two E_u (D_{4h}) configurations $^1(a_{1u}e_g)$ and $^1(a_{2u}e_g)$.[35] These two configurations add in a ~1:1 and out-of-phase fashion yielding a very-weakly-allowed state $Q = [(a_{1u}e_g) - (a_{2u}e_g)]/2^{1/2}$. The more intense Q(0,0) band of metallo-OEP monomers is understood by a small splitting (loss of degeneracy) of the $^1(a_{1u}e_g)$ and $^1(a_{2u}e_g)$ configurations and incomplete cancellation of the transition moments. The Q(1,0) band of both OEP and TPP monomers gains intensity via vibronic coupling with the strong Soret transition, which represents the allowed in-phase linear combination $B = [(a_{1u}e_g) + (a_{2u}e_g)]/2^{1/2}$.[24,35]

(39) Equations 4, and others given later in the text, indicate the major compositions of the states and should not be taken to imply that the true eigenstates of the complexes will contain equal admixtures of the appropriate configurations. For example, the *net* CT character of the eigenstates will depend on the relative contributions of the opposing CT configurations to the CR configurations, which will differ for the symmetric and asymmetric complexes.

where the "center of gravity" of the mono(porphyrin) Q and B states is

$$E_m = \Delta\epsilon - (a_{1u}^A a_{1u}^A | e_g^A e_g^A) + 2(a_{1u}^A e_g^A | a_{1u}^A e_g^A) \quad (6)$$

and $\Delta\epsilon$ is the mono(porphyrin) HOMO-LUMO gap (Appendix 1).

It is seen from eqs 4a and 4b that the B^+ and Q^+ states represent in-phase exciton components, both being comprised in the simple model solely of locally-excited configurations with no CT contribution. The B^+ state gives rise to an intense absorption shifted to the blue of the B band of mono(porphyrin) complexes by the last term in eq 5a.[40] The Q^+ energy predicted by our eight-orbital model is the same as that predicted for Q(0,0) by the four-orbital model of mono(porphyrin) complexes,[24,35] thus giving semiquantitative agreement with the experimental results for the symmetric complexes such as $Th(TPP)_2$ and validity to the model and its a priori assumptions.

The model also delineates the origin of the Q″ absorption feature located between the mono(porphyrin)-like Q and B bands (Figures 1 and 2). We assign this feature to the two CR^+ states, CR_1^+ and CR_2^+.[41] This assignment is consistent with the observation that the Q″ band shifts to the red and intensifies as the rings are brought closer together by decreasing the ionic radius of the metal ion. The bathochromic spectral shift is associated with the increased Coulomb stabilization of the parent CT and hence CR configurations with decreasing macrocycle separation (via the second term in eqs 5c and 5d), and the increased intensity is due to increased orbital overlap.

The existence of two essentially pure CR states (CR_1^+ and CR_2^+) containing only contributions from the two parent CT configurations and no contribution from the parent locally-excited configurations is a direct result of the spectrally-demanded generation of two states (B^+ and Q^+) with just the opposite electronic parentage. The formation of these relatively pure states is a direct consequence of the degeneracy that we assumed for the diagonal terms in the E_1 CI matrix (Appendix 1) which results in the equal contribution of the four basis configurations to the eigenfunctions. Again, near-degeneracy of the a_{1u}- and a_{2u}-derived configurations is a good approximation for the symmetric TPP-substituted sandwich complexes such as $Th(TPP)_2$. The degeneracy will be lost to some extent in the symmetric OEP-substituted complexes such as $Th(OEP)_2$ and thus have the effect of introducing increased mixing between the B^+/Q^+ and CR^+ configurations. Empirically, an intermediate case (i.e., partial recovery of the degeneracy) seems to occur for the asymmetric complexes such as Th(OEP)(TPP), where the intensity of the Q(0,0) band is low and close to that of $Th(TPP)_2$ (Figures 1 and 2).

This analysis and the assignment of the CR^+ states as giving rise to the Q″ feature in the ground state absorption spectrum provide crucial empirical evidence that the parent CT configurations of porphyrins within van der Waals contact lie close in energy to those of the parent locally-excited configurations. The analysis places the ^1CR configurations ~0.4 eV higher than the Q(0,0) energy of $Th(TPP)_2$ and, furthermore, only ~0.1 eV above the parent $^1(a_{1u}e_g)$ and $^1(a_{2u}e_g)$ configurations when it is considered that configuration interaction in mono(porphyrin) complexes is responsible for Q(0,0) being energetically below (and B(0,0) above) the energy E_m of these configurations. At the shorter intermacrocycle separation ($R_{mean} \sim 3.2$ Å) of $Hf(TPP)_2$ and $Zr(TPP)_2$,[9,10] the Q′ band lies at 505 nm (Figure 2),[16] which gives the parent CT configurations an energy slightly lower than E_m. These results are important since the lack of direct information on the energies of the CT configurations of the reaction center special pair,[2,3] simple porphyrin dimers,[34] excimers and paracyclophanes,[5,6] and other systems has led to uncertainty in assessment of the electronic properties of these molecules. Our findings on the porphyrin sandwich complexes provide support for the proposal that the CR (and parent CT) configurations of the reaction center special pair have energies comparable to the Q_Y states of the chromophores.[2b,d,32,42]

Singlet Electronic States Derived from the Dipole-Forbidden E_3 Configurations: The Low-Energy Q′ and Higher-Energy States. The four E_3 (e.g. E_{3y}) configurations do not exhibit the near-degeneracy of the E_1 configurations (see dashed arrows in Figure 7). In particular, the configurations derived by electron promotion from the antibonding HOMOs (a_1 and a_2) to the bonding LUMO (e_3) should have much lower energy than those involving the b_2 and b_1 bonding HOMOs and antibonding e_1 LUMO. However, near-degeneracy is preserved *within* the a_{1u}- and a_{2u}-derived *pairs* of configurations $(a_1e_3)/(a_2e_3)$ (short dashed arrows in Figure 7) and $(b_2e_1)/(b_1e_1)$ (long dashed arrows). The resulting singlet E_3 CI matrix, eigenfunctions, and eigenvalues are given in Appendix 2. Expressing the eigenfunctions in terms of the exciton/CR basis gives

$$\psi^{\pm} = [(1 + \lambda_{\pm})Q^- + 2^{-1/2}(1 - \lambda_{\pm})(CR_1^- - CR_2^-)]/[2(1 + \lambda_{\pm}^2)]^{1/2} \quad (7a)$$

$$\phi^{\pm} = [(1 + \eta_{\pm})B^- + 2^{-1/2}(1 - \eta_{\pm})(CR_1^- + CR_2^-)]/[2(1 + \eta_{\pm}^2)]^{1/2} \quad (7b)$$

with $\lambda_{\pm}$ and $\eta_{\pm}$ dependent on the resonance integral β (eqs A11), and

$$\begin{aligned} B^- &= [(b_1e_1) + (b_2e_1) + (a_2e_3) + (a_1e_3)]/2 \\ &= [a_{1u}^A e_g^A + a_{2u}^A e_g^A - a_{1u}^B e_g^B - a_{2u}^B e_g^B]/2 \\ &= [B^A - B^B]/2^{1/2} \end{aligned} \quad (8a)$$

$$\begin{aligned} Q^- &= [(b_1e_1) - (b_2e_1) + (a_2e_3) - (a_1e_3)]/2 \\ &= [a_{1u}^A e_g^A - a_{2u}^A e_g^A - a_{1u}^B e_g^B + a_{2u}^B e_g^B]/2 \\ &= [Q^A - Q^B]/2^{1/2} \end{aligned} \quad (8b)$$

$$\begin{aligned} CR_1^- &= [a_{1u}^A e_g^B - a_{1u}^B e_g^A]/2^{1/2} \\ &= [CT_1^{AB} - CT_1^{BA}]/2^{1/2} \end{aligned} \quad (8c)$$

$$\begin{aligned} CR_2^- &= [a_{2u}^A e_g^B - a_{2u}^B e_g^A]/2^{1/2} \\ &= [CT_2^{AB} - CT_2^{BA}]/2^{1/2} \end{aligned} \quad (8d)$$

where again CT_1^{AB} etc. are the parent CT configurations.

We associate Q′ with ψ^- and thus associate the lowest energy of these dipole-forbidden E_3 states with the red-region ground-state absorption of the sandwich complexes.[16] This assignment is consistent with the weakness of this absorption and the large shift between the Q′ absorption and emission maxima in Figure 4. We have argued previously that the Q′ state is essentially dipole forbidden and that the Q′ absorption/emission intensity is derived from vibronic coupling with the Soret transition (see also below).[15,16] Additionally, the partial CR^- character of Q′ is consistent with the observation that the Q′ absorption shifts to longer wavelengths as the ionic radius of the metal decreases and the intermacrocycle overlap increases (Figure 2) due to (i) stabilization of the CR (and parent CT) configurations and (ii) an increase in β (eq A12a).

It is obvious from eqs 7 that the four E_3 singlet states, unlike the four E_1 singlet eigenstates, have substantially mixed exciton and CR character. The degree of mixing depends on both the magnitude of the matrix elements and the energy gap (4β) between the a_{2u}-derived basis functions (a_1e_3) and (b_2e_1) and between the

(40) The four two-electron integrals in eq A3 add in phase and give rise to the last term in the expression for $E(B^+)$ in eq 5a which is responsible for the exciton shift of the Soret band in the sandwich complexes. The four terms in eq A3 add destructively and cancel in the expression for $E(Q^+)$ in eq 5b, which is equivalent to there being no exciton splitting involving the Q states of the porphyrin subunits in the limit that the Q bands have no intensity (i.e. if the a_{1u}- and a_{2u}-derived configurations are exactly degenerate and have equal transition moments).

(41) These states will split in energy if the degeneracy between the a_{1u}- and a_{2u}-derived configurations is lifted. In fact, the CR_1^+ and CR_2^+ states may give rise to the splitting in the Q″ band observed in the low-temperature spectrum of $Th(OEP)_2$ (Figure 3). Therefore, we have not generated eigenstates by taking linear combinations of CR_1^+ and CR_2^+ even with the assumed degeneracies in the simple zeroth-order model.

(42) DiMagno, T. J.; Bylina, E. J.; Angerhofer, A.; Youvan, D. C.; Norris, J. R. *Biochemistry* **1990**, *29*, 899–907.

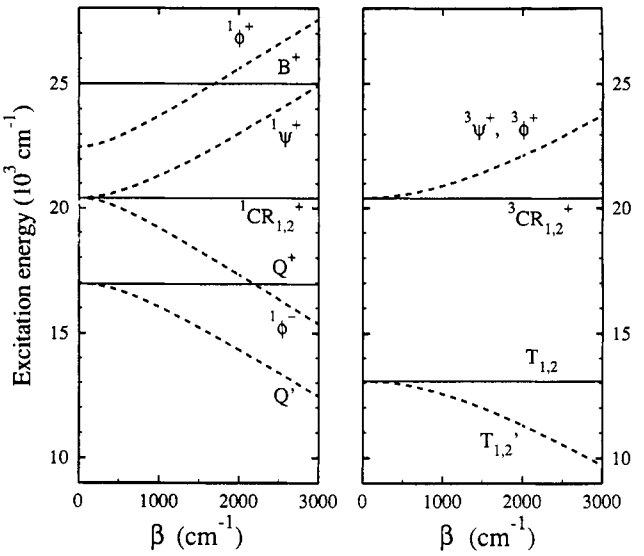

Figure 8. Excitation energies of the idealized bis(porphyrin) singlet (left panel) and triplet (right panel) eigenstates derived in the text as a function of the intermolecular resonance integral, β, in cm^{-1}. Dashed lines denote the dipole-forbidden E_3 configurations (those with mixed EX/CR character) and solid lines correspond to the E_1 dipole-allowed states which retain relatively pure EX or CR character in the model.

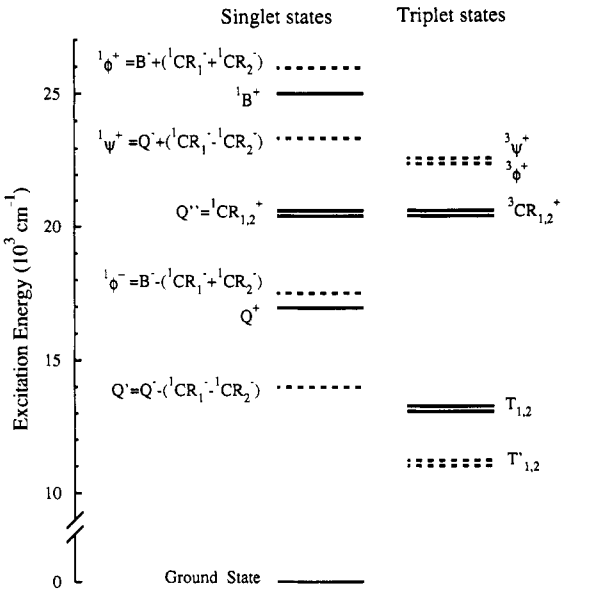

Figure 9. State diagram showing the excitation energies and parentage of the singlet (left side) and triplet (right side) excited states obtained via the model outlined in the text using β = 0.27 eV. Dashed lines are used for the E_3 states and solid lines are used for the E_1 states. The wave functions displayed are intended to indicate the parentage of the states in the EX/CR basis and should not be taken to suggest an equal admixture of the contributing configurations.

a_{1u}-derived basis functions (a_2e_3) and (b_1e_1). Thus, the existence of states with *mixed* parentage can be traced directly to the *nondegeneracy* of the appropriate E_3 basis configurations. For the E_1 states it is the *degeneracy* of the two a_{1u}-derived and of the two a_{2u}-derived configurations that yields relatively *uncoupled* exciton and CR states.[43]

The Empirically-Derived Intermolecular Resonance Integral β and the Energies/Composition of the E_3 Eigenstates. In Appendix 3, it is shown that the spectroscopic data combined with our model lead to an estimate of $\beta \sim 0.27$ eV.[44] This value of β is comparable to those calculated for paracyclophanes thought to have macrocycle spacings similar to the ~3.5-Å distance between the core atoms of the Th sandwich complexes.[5a,6b] The derived β permits estimates of the energies and composition of the E_3 eigenstates via eqs 7, A11, and A12. The composition of the Q′ state ψ^- is found to be roughly 60% Q$^-$ and 40% CR$^-$. This shows that the sandwich complexes are indeed strongly-coupled systems. The energies of the eigenstates vary with β as shown in Figure 8, and from these plots many of the spectroscopic energies can be estimated in terms of this single parameter. The state energies obtained using β = 0.27 eV are shown in Figure 9.

On the basis of our analysis, it is likely that the remaining three E_3 states ψ^+ and $\phi^\pm$ have energies greater than the Q$^+$ = Q(0,0) energy and contribute to the broad weak absorption between the Soret and Q bands. Indeed, in the spectra of Hf(TPP)$_2$, Zr(TPP)$_2$ (Figure 2),[9,10,16] Th(OEP)$_2$, and Th(OEP)(TPP) at 78 K (Figure 3) several features are observed in this region in addition to the Q″ band assigned to the two E_1 states CR_1^+ and CR_2^+. Our assignments of the E_3 states are self-consistent in placing both the CR$^+$ and CR$^-$ configurations slightly above Q(0,0) in energy.

This analysis and the conclusion that the ψ^- = Q′ state has substantially mixed Q$^-$ exciton and CR$^-$ character argues that the red-shift in the Q′ absorption from the monomer Q position is due to mixing of the exciton (or parent locally-excited) configurations with the CR (or parent CT) configurations at higher energy. A similar mechanism has been proposed to explain the red-shifted low-energy absorption of aromatic excimers.[5b-d] This mechanism is also thought to contribute to the reduced energy of the lowest excited state of the reaction center special pair, although exciton splitting is also expected to be significant due to the large dipole strength of the Q_y transitions of the bacteriochlorophyll subunits.[2,3] (Protein effects also may contribute to the red shift.) On the other hand, as noted above, insignificant exciton splitting is expected for the sandwich complexes investigated here due to the weak nature of the Q transitions of the porphyrin subunits. Hence, our observations and analysis of the electronic character of the $^1Q'(\pi,\pi^*)$ excited state of the simple porphyrin sandwich complexes support the proposal from theoretical studies[2a,b,3] and Stark-effect measurements[42,45] that mixing of the CT and Q_y configurations of the special pair contributes substantially to the spectral properties of the photoactive excited state of this complex.

The Absorption/Fluorescence Gap. The substantial (3000–4000 cm^{-1}) shift between the Q′ absorption and fluorescence maxima of the sandwich complexes (Figure 4) is explained by the model. The transitions should be weak, as is found, because the Q′ state is assigned as being a dipole-forbidden E_3 state ψ^-. The main, but weak, absorption/emission intensity may be derived from vibronic coupling of Q′ with the intense Soret (B) transition (or possibly with the Q transition) and thus should not occur at the state origin.[15,16] Thus, the underlying composition of the Q′ absorption and emission is likely to be quite complex in view of the large number of modes that may participate in vibronic borrowing in the sandwich complexes. This may explain in part the breadth of the features.

Another factor may also contribute to the breadth of the absorption/fluorescence gap and to the Q′ absorption and emission features. We expect that there will be more π–π bonding between the two porphyrin rings in the excited-state Q′ than in the ground state. This is because in the Q′ excited state, to a first approx-

(43) From another perspective, it is seen that in the weak coupling limit ($\beta \to 0$ and thus $\lambda_\pm$ and $\eta_\pm \to \mp 1$) $\psi^\pm$ and $\phi^\pm$ extrapolate to being relatively uncoupled exciton and CR states. In the strong coupling limit ($\beta \to \infty$), the states approach having 50/50 exciton/CR character. Thus, as the energetic splitting between the supermolecule HOMOs (β_1, β_2) and between the LUMOs (β_e) increases, mixing among the relevant E_3 configurations [e.g., (a_1e_3) and (b_2e_1)] will *decrease* and the mixed EX/CR parentage of the states will *increase*.

(44) The value of $\beta \sim 0.27$ eV is about a factor of two smaller than would be estimated on the basis of the ~1200–1300-nm position of the NIR transition in the oxidized sandwich complexes. In the simple model,[11e,17,18] the NIR transition would occur at an energy corresponding to 2β, the gap between the filled bonding HOMO and the half-filled antibonding LUMO of the dimer. The discrepancy between the values is likely due in part to the two-electron terms (Coulomb integrals) that also contribute to the energies of the electronic states of the dimer cations and thus to the NIR transition energy.

(45) (a) Lockhart, D. J.; Boxer, S. G. *Biochemistry* **1987**, *26*, 664–668, 2958 (correction). (b) Loesch, M.; Feher, G.; Okamura, M. Y. *Proc. Natl. Acad. Sci. U.S.A.* **1987**, *84*, 7537–7541.

imation, an electron has been transferred from a π–π antibonding orbital to a π–π bonding orbital. This additional π–π interaction in the excited state would cause the two macrocycles to move closer together following excitation, as has been discussed for various oxidized porphyrin sandwich complexes,[17,18] aromatic excimers,[5e] paracyclophanes,[6d,e] and the reaction center special pair.[4c,17c,32,46] A shorter porphyrin–porphyrin distance in the excited state vs the ground state raises the possibility that the Q′ band may consist of a progression built on one or more low-frequency modes as in the paracyclophanes[6d,e] and the reaction center special pair.[47,48] Although the symmetric inter-porphyrin "accordion" mode, for example, would not be vibronically active in D_{4d} symmetry, vibronic intensity may result from the slight deviations from D_{4d} symmetry exhibited by the sandwich complexes or via combinations with other modes. Alternatively, the dipole-forbidden E_3 state Q′ may derive intensity from the allowed E_1 states B or Q via vibronic coupling with one or more of the monomer-like out-of-plane deformation modes. Along these lines, the spectra of $Th(OEP)_2$ and Th(OEP)(TPP) in Figure 4 can be simulated reasonably well using a simple Franck–Condon progression built on an origin at ~710 nm with an inter-porphyrin mode having υ_{ground} = 200 cm^{-1} and $\upsilon_{excited}$ = 250 cm^{-1}, a Huang-Rhys (origin-shift) factor S = 6.1 for $Th(OEP)_2$ and 6.9 for Th(OEP)(TPP), and an inhomogeneous broadening of 300 cm^{-1} to wash out the progression into the observed broad Q′ absorption and emission features. These parameters are comparable to those used to describe the NIR vibronic progression of the oxidized sandwich complexes[17b,c] and are somewhat larger, as expected, than those derived for the excited special pair.[47]

The Triplet Manifold and Phosphorescence Spectra. The eigenfunctions and energies for the triplet electronic states of the sandwich complexes are similarly derived within our model.[28b] In fact, the triplet interaction matrices for the sandwich complexes are simpler than those for the singlets, as in mono(porphyrin) complexes,[24,35b] because CI between the analogous triplet a_{1u}- and a_{2u}-derived configurations is zero in D_{4d} symmetry. For example, the orbitally-allowed a_{1u}-derived E_1 triplet states are found to be a monomer-like exciton state T_1 and a CR state:

$$T_1 = [^3(b_1e_3) + {}^3(a_2e_1)]/2^{1/2} = [a_{1u}{}^Ae_g{}^A + a_{1u}{}^Be_g{}^B]2^{1/2} \quad (9a)$$

$$^3CR_1{}^+ = [^3(b_1e_3) - {}^3(a_2e_1)]/2^{1/2} = [a_{1u}{}^Ae_g{}^B + a_{1u}{}^Be_g{}^A]2^{1/2} \quad (9b)$$

Since the a_{1u} and a_{2u} orbitals of the subunits are assumed to be degenerate in the simple model, the corresponding a_{2u}-derived exciton and CR triplets, T_2 and $^3CR_2{}^+$ will be isoenergetic with T_1 and $^3CR_1{}^+$, respectively. As in the case of the E_1 singlets, it is the degeneracy *within* the a_{1u}- and a_{2u}-derived pairs of configurations that is responsible for the formation of relatively pure triplet exciton and CR states. The two $^3CR^+$ states are expected to be essentially isoenergetic with the two $^1CR^+$ states (Figures 8 and 9), due to negligibly small two-electron intermolecular exchange integrals.[33] We have assigned $^1CR_1{}^+/^1CR_2{}^+$ as giving rise to the Q″ absorption between the Soret and Q bands in the ground-state absorption spectrum. Thus, $^3CR_1{}^+$ and $^3CR_2{}^+$ are high-energy triplets which should relax rapidly to the lower-energy triplets.

The triplet states T_1 and T_2 are expected to have energies comparable to those of mono(porphyrin) triplets since exciton coupling between the subunit triplets is expected to be very small. Since the phosphorescence of lanthanide OEP mono(porphyrin) complexes occurs near 700 nm,[24] and no emission is observed at this short a wavelength for the OEP-containing Th bis(porphyrin) sandwich complexes (Figures 5, B and C), it appears that phosphorescence from T_1 and T_2 is not significant.[49]

The main emission from the Th bis(porphyrin) sandwich complexes at ambient temperature is the phosphorescence occurring between 900 and 1000 nm (Figure 5). This emission can be understood by examining the orbitally-forbidden E_3 triplet states, in analogy with the low-energy $^1Q'$ absorption/fluorescence. Again, the problem simplifies to consideration of a pair of a_{1u}-derived configurations, $^3(a_2,e_3)$ and $^3(b_1,e_1)$, separated by 4β, and a pair of a_{2u}-derived configurations, $^3(a_1,e_3)$ and $^3(b_2,e_1)$, also separated by 4β. This splitting leads to the appearance of red-shifted orbitally-forbidden T_1' and T_2' states (which are degenerate in the simple model), in analogy with the Q′ (ψ^-) state in the singlet manifold. Continuing the analogy, the T′ triplets, as well as the higher-energy E_3 triplets $^3\psi^+$ and $^3\phi^+$, have both substantial exciton and CR character. With use of $\beta \sim 0.27$ eV obtained above from the red shift of Q′ relative to Q in the singlet manifold, the model predicts that the T′ states have ~70/30 exciton/CR character and vice versa for the $^3\psi^+$ and $^3\phi^+$ states. In further analogy with the singlet manifold, this mixing contributes substantially to the lower energy of T_1' and T_2' compared to the monomer-like T_1 and T_2 states (Figures 8 and 9).

The model predicts a red shift of ~0.25 eV (2050 cm^{-1}).[28b] Relative to the 764-nm emission[23] of $Th(TPP)(acac)_2$, this places the T′ phosphorescence of $Th(TPP)_2$ near 900 nm, in good agreement with the data (Figure 5A). The agreement is not as good for the OEP-containing complexes; this is expected since the assumed degeneracy of the a_{1u}- and a_{2u}-derived configurations is less valid. Additionally, we suspect that the main phosphorescence between 900 and 1000 nm for the three complexes may not represent the origin of the T′ states (Figure 5). The reasoning is analogous to that used above to account for the spectra of the fluorescent Q′ singlet state (Figure 4), which is also an orbitally-forbidden E_3 state having mixed exciton/CR parentage. Furthermore, the activation energy of ~1700 cm^{-1} estimated from the temperature dependence of the delayed fluorescence of $Th(OEP)_2$ along with an electronic origin for the Q′ excited state near 710 nm (the average position of the Q′ absorption and emission maxima) places the T′ phosphorescence origin near 810 nm, which is to the blue of the observed maximum.

Additional complexity is expected since there are two close-lying a_{1u}- and a_{2u}-derived triplets T_1' and T_2'. Furthermore, there may be multiple conformers, perhaps derived from the peripheral groups on the macrocycles, as has been suggested to account for the vibronic contour of the NIR band of the oxidized lanthanide sandwich complexes.[17b,18c] These factors may contribute to the complexity of (i) the temperature dependence of the low-energy region of the phosphorescence, where a shoulder is seen most clearly for $Th(TPP)_2$ (Figure 5), and (ii) the triplet state decay (ground-state recovery) kinetics, where the OEP-containing complexes show clear indications of nonexponential behavior (especially at 77 K) whereas $Th(TPP)_2$ does not. Despite these complexities, our model provides a very reasonable picture of the triplet manifold and the associated phosphorescence behavior of the sandwich complexes.

Excited-State Absorption. Finally, the model is successful in explaining the overall characteristics of the excited-state absorption spectra. The most likely visible/NIR transitions initiated from the fluorescent Q′ state are to states B^+ and Q″ (Figures 8 and 9). Recall that Q′ has Q^- exciton and CR^- character, B^+ is basically an exciton state, and Q″ has mainly $CR_1{}^+/CR_2{}^+$ character. The relative strengths of these transition can be evaluated from

(46) Warshel, A. *Proc. Natl. Acad. Sci. U.S.A.* **1980**, *77*, 3105–3109.
(47) (a) Johnson, S. G.; Tang, D.; Jankowiak, R.; Hayes, J. M.; Small, G. J. *J. Phys. Chem.* **1990**, *94*, 5849–5855. (b) Middendorf, T. R.; Mazzola, L. T.; Gaul, D. F.; Schenck, C. C.; Boxer, S. G. *J. Phys. Chem.* **1991**, *95*, 10142–10151.
(48) (a) Donohoe, R. J.; Dyer, R. B.; Swanson, B. I.; Violette, C. A.; Frank, H. A.; Bocian, D. F. *J. Am. Chem. Soc.* **1990**, *112*, 6716. (b) Bocian, D. F. *Proc. SPIE* **1991**, *1432*, 166. Shreve, A.; Cherepy, N.; Franzen, S.; Boxer, S. G.; Mathies, R. A. *Proc. Natl. Acad. Sci. U.S.A.* **1991**, *88*, 11207–11211.

(49) However, since the phosphorescence from $Th(TPP)(acac)_2$ occurs at 764 nm,[23] we cannot rule out the possibility that (delayed) phosphorescence from the monomer-like states T_1 and T_2 makes some contribution to the broad shoulder observed in this region for $Th(TPP)_2$ (Figure 5A). This shoulder and the corresponding emission observed near 800 nm for the OEP-containing complexes in degassed solution was attributed above mainly to delayed fluorescence.

$$\langle B^+|-e\sum z_i|Q'\rangle = [(\lambda_- - 1)/(1 + \lambda_-^2)^{1/2}][\langle b_1|-ez|a_2\rangle - \langle e_3|-ez|e_1\rangle - \langle b_2|-ez|a_1\rangle + \langle e_3|-ez|e_1\rangle] \approx 0 \quad (10a)$$

$$\langle CR_1^+|-e\sum z_i|Q'\rangle = [(1 + \lambda_-)/(1+ \lambda_-^2)^{1/2}][\langle b_1|-ez|a_2\rangle + \langle e_3|-ez|e_1\rangle] \quad (10b)$$

$$\langle CR_2^+|-e\sum z_i|Q'\rangle = [-(1 + \lambda_-)/(1 + \lambda_-^2)^{1/2}][\langle b_2|-ez|a_1\rangle + \langle e_3|-ez|e_1\rangle] \quad (10c)$$

Although these $E_3 \rightarrow E_1$ transitions are symmetry allowed (z-polarized), the $Q' \rightarrow B^+$ transition is predicted to be very weak due to cancellation of the a_{1u}- and a_{2u}-derived terms. In view of eqs 10b and 10c, the $Q' \rightarrow Q''$ (i.e. $Q^-/CR^- \rightarrow CR^+$) transition is expected to have an intensity comparable to the NIR band in the oxidized sandwich complexes; the latter is thought to be associated with electron promotion from a bonding HOMO (b_1 or b_2) to a half-filled antibonding HOMO (a_1 or a_2).[11e,17,18] Although the $Q' \rightarrow Q''$ absorption maximum and origin have not been resolved, estimates can be made from the Q''/Q' spacing in the ground-state absorption spectra. For example, the predicted wavelength of 1320 nm for the electronic origin is in accord with the observation that the Q′ excited-state absorption spectra of $Zr(TPP)_2$ and $Hf(TPP)_2$ has a prominent absorption past 1000 nm.[16,28] A difference between the predicted transition origin and the location of the main absorption intensity is not unreasonable since the $Q' \rightarrow Q''$ transition may be accompanied by a change in the inter-porphyrin distance, as discussed above and elsewhere[16] for the transition from the ground state to Q′ and previously[17] for the NIR absorption of the oxidized species. The $Q' \rightarrow Q''$ transition for the Th bis(porphyrin) sandwich complexes is expected to occur past 1500 nm (well beyond our detection limit), due to the larger spacing between the macrocycles. Hence, our model also accounts for the featureless Q′ excited-state absorption spectrum in the visible/NIR region for the Th bis(porphyrin) sandwich complexes. Additionally, the very weak feature seen near 890 nm in the ~1-ps transient spectrum of $Th(OEP)_2$ in Figure 6 is at an appropriate energy for the $Q' \rightarrow B^+$ transition and has the low oscillator strength predicted by eq 10a.

The triplet–triplet excited-state absorption spectra may be analyzed in a similar manner. The transition from T′ (the phosphorescent state having both exciton and CR^- character) to the $^3CR^+$ states is dipole allowed ($E_3 \rightarrow E_1$), similar to the excited singlet $Q' \rightarrow Q''$ absorption. The energy of the $^3CR^+$ triplets can be estimated from the position of the Q″ ($^1CR^+$) ground-state absorption, since the singlet and triplet CR^+ states are expected to lie close in energy. Thus, for $Th(OEP)_2$, for example, the $T' \rightarrow {}^3CR^+$ transition is predicted to occur near 1100 nm, in good agreement with the intense absorption to the red of ~1000 nm (Figure 6).

Conclusion

The static and time-resolved optical absorption and emission data for the thorium bis(porphyrin) sandwich complexes studied here, as well as for other complexes investigated previously, have been interpreted with a relatively simple model for the electronic states of these strongly-coupled systems. The model extends the mono(porphyrin) four-orbital model to a cofacial bis(porphyrin) system and is consistent with all the key optical characteristics of the porphyrin sandwich complexes: (i) the presence of monomer-like Q and B bands, (ii) new weak, low-energy Q′ absorption and emission bands that are several thousand wavenumbers below the Q(0,0) band, (iii) new Q″ absorption bands between the Q and B bands, (iv) prominent NIR excited-state absorption, and (v) red-shifted phosphorescence bands. The red-shifted absorption, fluorescence, and phosphorescence arise from states that acquire an increased amount of charge resonance character as the electronic interactions between the porphyrins become stronger. We propose that the Q″ state has predominantly charge resonance character. This provides an estimate for the energy of the parent charge transfer configurations in these systems. The spectroscopic results and analyses presented here on the well-defined sandwich complexes provide a more detailed understanding of the excited states and optical properties of paired π-systems held within van der Waals contact, including the reaction center special pair.

Acknowledgment. This work was supported in part by Grants GM34685 and HL25934 from the National Institutes of Health. Receipt of an NIH Career Development Award (K.S.S.), a Sloan Foundation Research Fellowship (G.S.G. and K.S.S.), and a Dreyfus Foundation Teacher–Scholar Award (G.S.G.) are gratefully acknowledged. We thank Dr. D. Bocian for helpful discussions.

Appendix 1. Interaction Matrix for the Singlet E_1 Configurations

Using the approximations noted in the text, the interaction matrix for the dipole-allowed singlet E_1 configurations is

H	(a_1e_1)	(a_2e_1)	(b_2e_3)	(b_1e_3)
(a_1e_1)	E	α	δ	α
(a_2e_1)	α	E	α	δ
(b_2e_3)	δ	α	E	α
(b_1e_3)	α	δ	α	E

where

$$\alpha = (a_{1u}{}^A e_g{}^A|a_{2u}{}^A e_g{}^A) + (a_{1u}{}^A e_g{}^A|a_{2u}{}^B e_g{}^B) \quad (A1)$$

$$\delta = (a_{1u}{}^A e_g{}^A|a_{1u}{}^A e_g{}^A) + (a_{1u}{}^A e_g{}^A|a_{1u}{}^B e_g{}^B) - [(a_{1u}{}^A a_{1u}{}^A|e_g{}^A e_g{}^A) - (a_{1u}{}^A a_{1u}{}^A|e_g{}^B e_g{}^B)]/2 \quad (A2)$$

and $(ab|cd) = \int\int a(1)b(1)e^2/r_{12}c(2)d(2)\, dv_1\, dv_2$. Equation A2 was obtained using

$$(a_{1u}{}^A e_g{}^A|a_{1u}{}^B e_g{}^B) \approx (a_{2u}{}^A e_g{}^A|a_{2u}{}^B e_g{}^B) \approx (a_{1u}{}^A e_g{}^A|a_{2u}{}^B e_g{}^B) \approx (a_{2u}{}^A e_g{}^A|a_{1u}{}^B e_g{}^B) \quad (A3)$$

which is reasonable on the basis of calculations for the Sn^{IV} bis(phthalocyanine) sandwich complexes.[33] If we assume that $\beta_1 \approx \beta_2 \approx \beta_e$, the energy of the degenerate singlet E_1 configurations relative to the ground state is

$$E = \epsilon_{e1} - \epsilon_{a2} - (a_2a_2|e_1e_1) + 2(a_2e_1|a_2e_1) = \Delta\epsilon - [(a_{1u}{}^A a_{1u}{}^A|e_g{}^A e_g{}^A) + (a_{1u}{}^A a_{1u}{}^A|e_g{}^B e_g{}^B)]/2 + (a_{1u}{}^A e_g{}^A|a_{1u}{}^A e_g{}^A) + (a_{1u}{}^A e_g{}^A|a_{1u}{}^B e_g{}^B) \quad (A4)$$

where ϵ_{e1} and ϵ_{a2} are the energies of the bis(porphyrin) e_1 and a_2 orbitals and

$$\Delta\epsilon = \epsilon_{eg} - \epsilon_{a1u} = \epsilon_{eg} - \epsilon_{a2u} \quad (A5)$$

is the mono(porphyrin) HOMO-LUMO energy gap (ϵ_{eg}, ϵ_{a1u}, and ϵ_{a2u} are the energies of the monoporphyrin orbitals). The singlet E_1 eigenfunctions are given by eqs 3 and 4. The energy eigenvalues are

$$E(B^+) = E + \delta + 2\alpha \quad (A6a)$$

$$E(Q^+) = E + \delta - 2\alpha \quad (A6b)$$

$$E(CR_1^+) = E - \delta \quad (A6c)$$

$$E(CR_2^+) = E - \delta \quad (A6d)$$

which can be reexpressed in terms of the exciton/CR basis as given by eqs 5.

Appendix 2. Interaction Matrix for the Singlet E_3 Configurations

Using the approximations noted in the text, the interaction matrix for the dipole-forbidden singlet E_3 configurations is

H	(a_1e_3)	(a_2e_3)	(b_2e_1)	(b_1e_1)
(a_1e_3)	$E' - 2\beta$	α'	δ'	α'
(a_2e_3)	α'	$E' - 2\beta$	α'	δ'
(b_2e_1)	δ'	α'	$E' + 2\beta$	α'
(b_1e_1)	α'	δ'	α'	$E' + 2\beta$

where

$$\alpha' = \alpha - 2(a_{1u}{}^{A}e_g{}^{A}|a_{2u}{}^{B}e_g{}^{B}) \quad (A7)$$

$$\delta' = \delta - 2(a_{1u}{}^{A}e_g{}^{A}|a_{1u}{}^{B}e_g{}^{B}) \quad (A8)$$

$$E' = E - 2(a_{1u}{}^{A}e_g{}^{A}|a_{1u}{}^{B}e_g{}^{B}) = E - 2(a_{2u}{}^{A}e_g{}^{A}|a_{2u}{}^{B}e_g{}^{B}) \quad (A9)$$

with α, δ, and E given by eqs A1, A2, and A4. The E_3 eigenfunctions are

$$\psi^{\pm} = \{[(a_2e_3) - (a_1e_3)] + \lambda_{\pm}[(b_1e_1) - (b_2e_1)]\}/[2(1 + \lambda_{\pm}{}^2)]^{1/2} \quad (A10a)$$

$$\phi^{\pm} = \{[(a_2e_3) + (a_1e_3)] + \eta_{\pm}[(b_1e_1) + (b_2e_1)]\}/[2(1 + \eta_{\pm}{}^2)]^{1/2} \quad (A10b)$$

where

$$\lambda_{\pm} = [2\beta \pm (4\beta^2 + (\delta' - \alpha')^2)^{1/2}]/(\delta' - \alpha') \quad (A11a)$$

$$\eta_{\pm} = [2\beta \pm (4\beta^2 + (\delta' + \alpha')^2)^{1/2}]/(\delta' + \alpha') \quad (A11b)$$

The eigenfunctions may be expressed in terms of the exciton/CR basis functions as shown in eqs 7 and 8. The singlet E_3 energy eigenvalues are

$$E(\psi^{\pm}) = E' - \alpha' \pm (4\beta^2 + (\delta' - \alpha')^2)^{1/2} \quad (A12a)$$

$$E(\phi^{\pm}) = E' + \alpha' \pm (4\beta^2 + (\delta' + \alpha')^2)^{1/2} \quad (A12b)$$

Appendix 3. Estimate for the Intermolecular Resonance Integral β

Equations A1–A3, A6b, 5b, A7, A8, and A12a yield for the red shift of the E_3 state $\psi^- = Q'$ relative to the monoporphyrin-like E_1 state $Q^+ = Q$

$$E_Q - E_{Q'} = (\delta - \alpha) + (4\beta^2 + (\delta - \alpha)^2)^{1/2} \quad (A13)$$

A value of 0.36 eV is estimated for the left-hand side of this equation using $E_{Q'} \approx 1.74$ eV from the 710-nm Q′ origin (the average of the Q′ absorption and emission maxima in Figure 4) and $E_Q \approx 2.10$ eV from the 590-nm Q(0,0) band position for $Th(TPP)_2$ (Figure 1). The term $(\delta - \alpha)$ on the right-hand side of eq A13 is obtained as follows. Equations A1–A3 may be manipulated to give

$$(\delta - \alpha) = (a_{1u}{}^{A}e_g{}^{A}|a_{1u}{}^{A}e_g{}^{A}) - [(a_{1u}{}^{A}a_{1u}{}^{A}|e_g{}^{A}e_g{}^{A}) - (a_{1u}{}^{A}a_{1u}{}^{A}|e_g{}^{B}e_g{}^{B})]/2 - (a_{1u}{}^{A}e_g{}^{A}|a_{2u}{}^{A}e_g{}^{A}) \quad (A14)$$

The first (intra-porphyrin exchange) integral on the right-hand side of eq A14 is $(a_{1u}{}^{A}e_g{}^{A}|a_{1u}{}^{A}e_g{}^{A}) \sim 0.445$ eV from the difference between the average Q/B energy ($\sim$2.51 eV) and the phosphorescence origin ($\sim$1.62 eV) for $Th(TPP)(acac)_2$.[23] The last (intra-porphyrin electron repulsion) integral may be estimated from the spacing of the Q(0,0) and B(0,0) bands of $Th(TPP)(acac)_2$ to be $(a_{1u}{}^{A}e_g{}^{A}|a_{2u}{}^{A}e_g{}^{A}) \sim 0.203$ eV. The term in square brackets in eq A14, which is the difference between the intra- and inter-porphyrin Coulomb integrals, is obtained in several steps. In analogy with analysis of mono(porphyrin) spectra,[35] the $Th(TPP)(acac)_2$ phosphorescence energy allows an estimate of $\Delta\epsilon - (a_u{}^{A}a_u{}^{A}|e_g{}^{A}e_g{}^{A}) \approx 1.62$ eV, where a_u is either the mono(porphyrin) a_{1u} or a_{2u} HOMOs and $\Delta\epsilon$ is the mono(porphyrin) HOMO/LUMO gap defined in eq A5. Substitution into the expression for the energy of either CR^+ eigenstate (eqs 5c or 5d), along with the 2.56-eV estimate for the energy of these (degenerate) states obtained from the 485-nm position of the Q″ (CR^+) absorption band of $Th(TPP)_2$ (Figure 1), yields $[(a_u{}^{A}a_u{}^{A}|e_g{}^{A}e_g{}^{A}) - (a_u{}^{A}a_u{}^{A}|e_g{}^{B}e_g{}^{B})] \sim 0.91$ eV. Thus, eq A14 gives $(\delta - \alpha) \sim -0.218$ eV. Substitution into eq 20 along with $E_Q - E_{Q'} \sim 0.36$ eV given above yields $\beta \sim 0.27$ eV for the intermolecular resonance integral.